Contribution of meandering rivers to natural carbon fluxes: Evidence from the Ucayali River, Peruvian Amazonia

Romain Walcker, Dov Corenblit, Frederic Julien, Jean-Michel Martinez, Johannes Steiger

Contribution of meandering rivers to natural carbon fluxes: evidence from the Ucayali River, Peruvian Amazonia

Romain Walcker[1], Dov Corenblit[2], Frédéric Julien[1], Jean-Michel Martinez[3], Johannes Steiger[2]

[1] Laboratoire Ecologie Fonctionnelle et Environnement, Université de Toulouse, CNRS, Toulouse, France.

[2] Université Clermont Auvergne, CNRS, GEOLAB, 63000 Clermont-Ferrand, France

[3] GET, Institut de Recherche pour le Développement, CNRS, Toulouse, France.

***Corresponding author:**

Romain Walcker, Porte 336, Bât. 4R1, Université de Toulouse, 118 route de Narbonne 31062, Toulouse, France.

Phone: +33-(0)5-61-55-89-27.

Fax: +33-(0)5-61-55-89-01.

E-mail: romain.walcker@univ-tlse3.fr

Journal: *Science of the Total Environment*

Paper type: Full papers

Keywords: Amazon; carbon; floodplain; forest age; meandering river; remote sensing;

Contribution of meandering rivers to natural carbon fluxes: evidence from the Ucayali River, Peruvian Amazonia

1. Abstract

Better understanding the fate of the atmospheric carbon (C) captured by plant photosynthesis is essential to improve natural C flux modelling. Soils are considered as the major terrestrial bioreactor and repository of plant C, whereas channel networks of floodplain rivers collect and transport, throughout the aquatic continuum, a significant part of plant primary production until its export through outgassing or sequestration in marine sediments. Here, we show that river meandering in forested floodplains is a crucial and widely overlooked Earth surface process promoting C fluxes from the atmosphere to the aquatic continuum, via the floodplain vegetation. Over a recent period of 35 years (1984-2019), we quantified those C fluxes in one of the most active meandering rivers on Earth, the Ucayali River, Peru, South America. We used map time series combined with above-ground forest C data to derive the amount of C that is annually captured by the growing floodplain vegetation within the active meander belt, as well as exported to the aquatic continuum by lateral channel erosion. We found that the annual building and erosion of forested floodplain areas was nearly balanced over time with $19.0\pm7.7\times10^3$ ha^{-1} yr^{-1} and $19.8\pm6.7\times10^3$ ha^{-1} yr^{-1}, respectively. While growing forests within the active meander belt annually captured $0.01\pm0.05\times10^6$ Mg C yr^{-1}, lateral channel erosion provided the nearly 100-fold amount of C to the river channel and its streamflow, i.e. $0.9\pm0.4\times10^6$ Mg C yr^{-1}. Our findings revealed that the migration of the Ucayali River channel provided nearly 10-times more lignified C per unit area to the aquatic continuum (44.7 ± 21.4 Mg C ha^{-1} yr^{-1}) than non-meandering central Amazonian floodplains do. Together, these findings point to the importance of quantifying the overall contribution of meandering rivers to natural C fluxes worldwide.

2. Introduction

Floodplains are areas of high primary production which provide fresh autochthonous carbon (C) to river waters through litterfall, plant and micro-organism respiration (Abril *et al.*, 2014). Levels of plant production in floodplains and the extent of the floodplain area can therefore considerably modulate the overall C quantity found in river waters (Ward *et al.*, 2017). Hence, floodplain vegetation, algae and floating macrophytes in highly productive and preserved tropical areas, directly and rapidly provide organic and inorganic C to rivers (Abril *et al.*, 2014; Sawakuchi *et al.*, 2017). Abril *et al.* (2014) further suggested that central Amazonian wetlands export half of their gross primary production to rivers, being the primary sources for CO_2 outgassing by the Amazon.

Over the last decade, several studies successively updated regional and global estimates of river C fluxes from land to oceans (Drake *et al*., 2018). These studies underscored large data gaps and uncertainties, suggesting that C fluxes might be much larger than previously thought. In particular, uncertainties in the contribution of wetlands and macrophytes as a source of C for rivers has been highlighted (Spencer *et al*., 2013) and the need for new investigations identified. Furthermore, river meandering, among other processes contributing to C input into rivers, river meandering remains however a largely overlooked Earth surface process (Peixoto *et al*., 2009). Yet, this process is recognized in sculpting the Earth surface since more than 5 centuries, and studies have recently pointed out its potential role in biogeochemical fluxes (Iepli & Lapôtre, 2019). Abiotic factors, like sedimentary dynamics in meandering rivers, have been suggested as essential than biotic factors, like productivity and respiration, in the terrestrial organic C cycle (Torres *et al.*, 2017; Ielpi & Lapôtre, 2019).

Typically, meandering rivers are characterized by lateral bank erosion occurring at the outer meander bends, whereas lateral accretion processes form point bars within inner meander bends (Leopold and Wolman, 1960; Allen, 1965). Within the Amazon basin, lateral channel migration generates meander scrolls forming a sequence of ridges and swales, on which a sequential primary forest succession of high productivity rapidly takes place (Salo *et al*., 1986; Junk *et al*., 1989; Puhakka *et al*., 1992). Forest succession, leading eventually to the mature stage, continues when the channel further migrates and point bars are integrated into the floodplain. Conversely, channel migration also causes bank erosion which in turn promotes direct massive inputs of coarse woody material to river channels, thus providing substantial quantities of autochthonous C, potentially exceeding those imported through litterfall and respiration. Active river meandering closely linked to point bar formation, floodplain aging and lateral channel erosion, thus presents a relevant Earth surface process to consider for accurately quantifying and understanding floodplain C sequestration and its export to the aquatic continuum (Wohl *et al*., 2013; Sutfin *et al*., 2016).

Here, we aimed to provide evidence that river meandering in Amazonian floodplains significantly contributes to river C budgets. Our objective was to quantify the amount of C that annually accumulates in the forest biomass, as well as the part that is annually exported to the river channel, within the active meander belt of the river, i.e. the area where contemporary channel migration occurred. We investigated one of the major active tributaries of the Amazon, the Ucayali River, Peru, over a period of 35 years (1984-2019). We used the yearly water classification history dataset provided by the Joint Research Centre to produce annual maps of point bar formation, floodplain ages and river channel erosion in the 1984-2019 active meander belt. Annual maps were combined with a model predicting the living above-ground forest C stock from the floodplain age to derive amounts of C annually fixed by net primary production and exported to river waters after bank erosion. The quantity, quality and fate of the C provided by Amazonian meandering rivers to the aquatic continuum is discussed in respect to the existing literature.

3. Method

3.1. Study area

The Ucayali River is located in the western part of the Amazon basin (Fig. 1a). It is a major tributary of the Amazon River extending approximately 900 km from its upstream confluence with the Rio Tambo and Rio Urubamba to its downstream confluence with the Marañón River. The mean annual water discharge is about 12 100 $m^3 s^{-1}$ and water depth between low and high flood flows can range from 8 to 15 m (Santini *et al.*, 2019). The maximum and minimum monthly flows, recorded over the 1996-2018 period at the Requena gauging station, is of 22 900 and 2 500 $m^3 s^{-1}$ respectively (HYBAM, 2020). Close to the town of Pucallpa, the floodplain width is about 25 km and the active meander belt is approximately 10 km in width (Fig. 1b, c). The Ucayali is considered as one of the last pristine free meandering white-water rivers worldwide, characterized by high suspended sediment loads, nutrient-rich waters and high lateral channel migration rates within an unconstrained, forested floodplain (Constantine *et al.*, 2014). Within meandering floodplain rivers, forest primary succession is distinctly age-zonated (Salo *et al.*, 1986; Junk *et al.*, 1989; Puhakka *et al.*, 1992). The vegetation succession progresses from early successional stages dominated by short-lived species to latter successional stages dominated by long-lived species along a cross-river and age gradient (Salo *et al.*, 1986; Lamotte, 1990; Fig. 2). The early stage of primary succession begins on newly formed alluvial bars, mainly point bars, rapidly colonized by *Tessaria integrifolia* L. and *Gynerium sagittatum*, forming dense canopies of about 5-8 m in height. This early pioneer stage is replaced by a second stage dominated by *Cecropia tessmannii*, forming a closed canopy of about 14-18 m in height. The *Cecropia* forest is located on older meander scrolls in backwater depressions. During these two first stages, vegetation contributes to sediment and organic matter trapping, which leads to floodplain construction and soil C sequestration (Fig. 2; Salo *et al.*, 1986). The following stage is a mixed forest dominated by *Ficus insipida* and *Cedrela odorata*, forming a closed canopy of about 20-25 m in height. At this stage, floodplain surface elevation is about 5 m above the low water level. Its topography is more homogeneous compared to the pioneer zone in the previous stages of succession. This is due to the deposition of large amounts of silt in backwater depressions during seasonal flooding. The later successional mixed forest is more diversified and composed of large trees with a canopy of about 40 m in height. Soil topography of the floodplain at this level (> 5-10 m above the low water level) is generally flat with only minor remaining depressions. This forest succession trajectory is basically the same at each meander of the Ucayali River (Kalliola *et al*., 1991). Lateral channel erosion leads to a continuous reset and regeneration of the primary vegetation succession over large areas (Salo *et al*., 1986; Kalliola *et al*., 1991). Since point bars of the Ucayali River are either rapidly eroded or integrated into the forested floodplain during lateral channel migration, we will, hereafter, exclusively distinguish the river channel from its floodplain, including point bars.

3.2. Mapping floodplain formation, aging and erosion

We used the yearly water classification history dataset (v1.2) provided by the Joint Research Centre (JRC) and freely available on the Google Earth Engine (GEE) platform (Gorelick *et al*., 2017). This dataset was firstly created by Pekel *et al.* (2016) and now consists in 36 annual raster maps spanning the 1984-2019 period. Pixels size approximately 900 m² at ground level and are classified in 'no data', 'non-water', 'seasonal water' or 'permanent water' (Fig. S1 in Appendix A). In order to create an envelope for data extraction, we firstly downloaded geometries (i.e. polylines shapefiles) of the Ucayali River from the Open Street Map database available at https://download.geofabrik.de. Then, we created a 10-km buffer across the river using the ArcGIS software package (ESRI, Redland, USA). The yearly water classification history dataset overlaying the river buffer was finally downloaded from the GEE platform. Using the MatLab software package (Mathworks, Natick, USA), the 36 annual raster maps were proceeded in order to map annual areas of floodplain formation, ages and erosion. The algorithm was applied pixel-by-pixel and year-by-year as illustrated in Figure 3. Pixels that were classified as ‘seasonal water’ or ‘permanent water’ at a given year (e.g. 1984; Fig. 3a), and classified ‘non-water’ the following year (e.g. 1985), were mapped as 1-year-old pixels. Each year from 1985 to 2019, every pixel age-determined at a given year (e.g. 1-year-old in 1985) and remaining ‘non-water’ the following year (e.g. 1986) was incremented with one additional year (e.g. 2-year-old in 1986). Remaining ‘non-water’ and ‘no data’ pixels with no age between successive years (e.g. between 1984 and 1985) were set to age ‘non-determined’ (ND). Typically, ND pixels corresponded to floodplain and upland areas created before 1984. Each year, from 1985 to 2019, every pixel age-determined at a given year (e.g. 2-year-old in 1986) and classified ‘seasonal water’ or ‘permanent water’ the following year (e.g. 1987) was considered as an eroded area (Fig. 3b) and reset to age 0 (e.g. 0-year-old in 1987).

3.3. Deriving C-stocks from floodplain ages

In line with Pahukka *et al.* (1992), we assumed that on the Ucayali River, pioneer vegetation colonizes bare alluvial bars from the year of their creation (Fig. S2 in Appendix A). We thus considered that the vegetation age is equal to the floodplain age. We used published data to predict the forest above-ground carbon stock (C-stock in Mg C ha^{-1}) from the floodplain age (age in years), and constructed a model predicting C-stock as a function of age (Fig. 3c). The data were published by Schöngart and Wittmann (2010) and based upon thousands of in situ vegetation structure inventories and tree ring measurements within floodplains of central Amazonia. Forest above-ground carbon stocks were estimated in several, almost undisturbed successional stages, with stands varying between 7 and 240 years of age. Forest structure data and several allometric models were used to construct a data series of C-stocks per forest age. First, we extracted data from the figure 18.10 presented by Schöngart and Wittmann (2010) using Web Plot Digitizer 4.3 software (Ankit Rohatgi, Pacifica, California, USA). Second, we fitted a 3rd order polynomial model to the 35 first years of the data series. These 35 years corresponded to the forest establishment that we analysed on the Ucayali River between 1984 and 2019. For floodplain forests established before 1984 (ND ages; Fig. 3a, b), we assumed a constant C-stock, i.e. old-growth forests with ages > 70-year-old in the data series. This assumption was based on the floodplain age structure of eroded outer meander bends presented in the results section.

3.4. Annual accumulation of floodplain forest C-stocks and its erosion

Floodplain areas were converted into above-ground forest C-stocks based on our model (Fig. 3c). The annual total C-stock (in Mg C ha^{-1}) was obtained by summing C-stocks of all vegetated floodplain ages since 1984. An annual C accumulation rate was obtained by (1) subtracting the total C-stock of year n by the one of year n-1, and (2) by applying a linear regression and the calculation of the root mean square error (RMSE). C-accumulation in floodplain and upland forest areas established before 1984 were not considered in the present study because they were outside of the 1984-2019 active-meander belt. Annual C-stock lost through floodplain erosion was obtained by summing eroded C-stocks of determined and non-determined (ND) floodplain ages.

4. Results

4.1. Annual vegetated floodplain area formation and erosion

Over the 1984-2019 period, the water surface area of the Ucayali River accounted for $220 \pm 25 \times 10^3$ ha (annual average and its standard deviation; Appendix B). Maximum water surface area extensions were observed in 1988, 1994, 2001, 2011, 2017 and minimums in 1987, 1992, 1997, 2005, 2010, 2013 and 2018 (Fig. 4a). Negative anomalies appeared mainly before 2000 and positives anomalies mainly after 2000. Yearly formation of floodplain areas occurred mainly within inner meander bends and accounted in average for $19.0 \pm 7.7 \times 10^3$ ha^{-1} yr^{-1} (Fig. 4b; Fig. 5; Appendix B and C). Conversely, floodplain erosion was located mainly in outer meander bends and closely balanced floodplain formation with an average of $19.8 \pm 6.7 \times 10^3$ ha^{-1} yr^{-1} (Fig. 4c; Appendix B and C).

4.2. Age structure of vegetated floodplain areas

We found that meandering promotes rejuvenation and recurrent formation of large areas of bare alluvial bars that are quickly colonized by pioneer vegetation. Over the 1984-2019 period, ages of floodplain areas were unevenly distributed (Fig. 6a). One-year-old floodplain areas largely dominated. However, about 1/3 of these newly formed floodplain areas were eroded the following year. Indeed, we found that older age classes generally decreased in areas following a negative logarithmic trend (Fig. 6a). This trend resulted from floodplain erosion (Fig. 6b). Newly established floodplain areas at inner meander bends were primarily affected by erosion at a rate of $6.4 \pm 3.3 \times 10^3$ ha^{-1} yr^{-1}, i.e. 1/3 of the yearly formed floodplain surface area ($19.0 \pm 7.7 \times 10^3$ ha^{-1} yr^{-1}). The rate of erosion decreased from younger to older floodplain areas (Fig. 6b). Floodplain erosion occurred equally in outer meander bends and in areas established before 1984, i.e. non-determined in age (ND) in the present study. Erosion in areas of ND ages accounted annually for about $7.0 \pm 3.8 \times 10^3$ ha^{-1} yr^{-1} (Fig. 6b; ND).

4.3. Annual changes in floodplain forest C-stocks

Our model used to derive C-stocks from floodplain ages showed a very good adjustment to the data ($R^2 = 0.99$; Fig. 7). One-year-old vegetation accounted for an average of 0.7 Mg C ha^{-1} and increased to 95.3 Mg C ha^{-1} at 35-year-old. Old-growth floodplain forests, i.e. those that established on areas older than 70-year-old, levelled off at nearly 115 Mg C ha^{-1} (Fig. 7). We combined annual maps of floodplain ages with our C-stock model and produced annual maps of above-ground C-stocks (Fig. 8). The mean annual C accumulation rate of floodplain forests established after 1984 in the Ucayali 1984-2019 active meander belt was estimated at 0.01×10^6 Mg C yr^{-1} with a RMSE of 0.04×10^6 Mg C yr^{-1} (Fig. 9a). Given the relation between available floodplain area and C-stock, the generation with the most effective C-sequestration capacity was the 23-year-old forest (Fig. 9b). Annual floodplain erosion caused by lateral channel migration accounted approximately for $0.9\pm0.4\times10^6$ Mg C yr^{-1} (Fig. 10a). Floodplain areas which established before 1984 largely dominated eroded C-stocks with $0.8\pm0.4\times10^6$ Mg C yr^{-1} (ND; Fig. 10b).

5. Discussion

5.1. Annual floodplain formation balances annual floodplain erosion in area but not in C budget

We found that rates of annual floodplain formation and rates of annual floodplain erosion appeared to be in balance over time with $19.0\pm7.7\times10^3$ ha^{-1} yr^{-1} and $19.8\pm6.7\times10^3$ ha^{-1} yr^{-1}, respectively. Our results confirm those reported by Puhakka *et al.* (1992) who showed that outer banks and point bars have, respectively, roughly equivalent rates of erosion and sediment deposition, maintaining a relatively constant channel width. Similarly, Peixoto *et al.* (2009) and Schwenk *et al.* (2017) reported an annual balance of erosion and deposition over large study areas and multidecadal periods. Peixoto *et al.* (2009) suggested that annual release of C caused by river dynamics would be much higher than the C annually sequestrated within the floodplain. Our results have quantitatively confirmed their hypothesis. Indeed, within the 1984-2019 active meander belt of the Ucayali River, the floodplain forest annually accumulates $0.01\pm0.04\times10^6$ Mg C yr^{-1} and exports $0.9\pm0.4\times10^6$ Mg C yr^{-1}. Although it appeared that there is a balance in areas between floodplain formation and erosion, we show that there is however a strong imbalance in rates of floodplain forest C fixation and export to river waters caused by lateral channel migration. This imbalance is mainly due to massive erosion of old-growth floodplain forests with high C-stock densities (about 115 Mg C ha^{-1}).

5.2. Lateral channel migration as a significant C provider to the aquatic continuum

There are multiple C sources for the aquatic continuum, i.e. between aquatic ecosystems from the atmosphere, headwater streams and inland waters, to coastal and marine systems. First, the C conveyed to streams and rivers can be provided during precipitation where water drops can be enriched in dissolved and particulate organic C (DOC, POC; Ward *et al.*, 2017). Then, when entering forest canopies, drops capture DOC and POC at the surface of leaves, branches and trunks. By instance, in the Rio Negro region, throughfall fluxes of 27.5 kg C ha^{-1} yr^{-1} have been reported (Filoso *et al*., 1999). Throughfall fluxes that range between 68.4 and 195.1 kg C ha^{-1} yr^{-1} and stem flow fluxes of 1.5 kg ha^{-1} yr^{-1} have been also reported in Amazonia (Neu et *al.*, 2016). In addition to the C provided by rainfall, root and canopy litterfall and respiration in floodplain forests together with algal and floating macrophyte communities are considered as the main C pathways to the aquatic continuum (Ward *et al*., 2017).

Even though they represent only about 14 % of the Amazon basin, floodplains are highly productive compared to terrestrial uplands and are hydrologically connected to river channels during yearly overbank flooding (Richey *et al.*, 1980; Junk, 1985; Hoffmann *et al*., 2009). It has been reported that in Central Amazonia, floodplains can provide an amount of 59.6 ± 38.7 Mg C ha^{-1} yr^{-1} to the channel network and streamflow (Abril *et al.*, 2014). Here, we point out that lateral channel erosion is a crucial and overlooked physical driver delivering large amounts of C to rivers. We show that channel migration in the upper Amazonian floodplain provides between 0.7 and 115 Mg C ha^{-1} yr^{-1} to streamflow depending on the age of the forested floodplain areas eroded. Over the studied period and area, we found that in average 44.7 ± 21.4 Mg C ha^{-1} yr^{-1} was delivered by lateral channel erosion to the aquatic continuum ($0.9\pm0.4\times10^6$

Mg C yr^{-1} delivered over $19.8 \pm 6.7 \times 10^3$ ha^{-1} yr^{-1}). Our result is roughly equivalent to the amount provided by the entire wetland system of the central Amazonian floodplain (i.e. flooded forest and macrophytes litterfall and respiration; 59.6 ± 38.7 Mg C ha^{-1} yr^{-1}), and roughly 10 times higher than the amount of the woody part considered by Abril *et al.* (2014) i.e. 5.3 ± 2 Mg C ha^{-1} yr^{-1}.

The amount of C provided by meandering rivers is dependant on annual rates of floodplain erosion. In the Amazon basin, different rates of channel migration of white-water rivers have been observed to exponentially increase from east to west (Kalliola *et al*., 1992; Mertes *et al*., 1995; Peixoto *et al.*, 2009; Salo and Räsänen, 1989). Therefore, inputs of woody materials as a consequence of lateral channel erosion may certainly increase along a downstream-upstream gradient. Further studies are thus required to quantify the spatial variability and overall contribution of Amazonian meandering rivers. Here, we have calculated the contribution of above-ground forest biomass to streamflow, but further amounts of C input may originate from (i) eroded floodplain soils (i.e. belowground total organic matter; Fig. 2), and (ii) the Andean mountains situated upstream the study area, where torrential streams potentially accumulate and transport large amounts of coarse woody debris provided by landslides occurring in particular during tropical storm events (McClain and Naiman, 2008; Clark *et al*., 2013; Wohl and Ogden, 2013).

5.3. Nature and fate of the C provided by meandering rivers

The nature of the C that is annually exported into the aquatic continuum is a fundamental aspect when considering the fate of this C and its role in the global cycle. It is usually considered that river C is advected downstream and returned to the atmosphere *via* degassing by both microbial and photochemical activity, ultimately resulting in a net zero exchange, especially in the tropics where warm temperatures stimulate organic matter decomposition (Raymond *et al.*, 2013; Ward *et al*., 2013). For instance, Abril *et al*. (2014) proposed that central Amazonian waters receive at least as much C from wetlands as they emit to the atmosphere, making a nearly neutral balance in atmosphere-biosphere CO_2 exchanges. However, the C provided by meandering rivers of the upper Amazon basin most probably differs from the C provided by wetlands of the central Amazon. On the one hand, it has been shown for wetlands of the central Amazon that the microbial communities decompose young organic C (> 5-year-old; Mayorga *et al.*, 2005; Abril *et al.*, 2014). On the other hand, the organic C found in the water column mainly originates from litterfall with low lignin content (Mayorga *et al*., 2005; Abril *et al.*, 2014). Our results suggest that in free meandering Amazonian rivers, such as the Ucayali River, older lignin is present in substantial quantities. Higher concentrations of lignin are found in tree trunks, branches and roots of ligneous terrestrial plants, and we estimated that mature and old growth floodplain forests accounted for nearly half of the eroded floodplain area within the Ucayali 1984-2019 meander belt (Fig. 6b). However, the fate of these large C quantities of lignin remains still uncertain. One hypothesis could be that this C is mineralized by microbial and photochemical activity and/or exported downstream the aquatic continuum and/or accumulated in the river sediment. Following Ward *et al.* (2013), half of these quantities could be degraded and mineralized in the Amazon River. Anyhow, according to Galy *et al.* (2015), the erosion and transportation capacities of rivers are to be considered as the main control of the biospheric C export to oceans. Many large water storage reservoirs have been recently proposed for the Amazon Basin (Finer and Jenkins, 2012). Since meandering rivers are known to be highly sensitive to the disruption of sediment supply caused by such engineering projects (Constantine et al, 2014), it is highly suspected that such human infrastructures will greatly alter the natural C fluxes we have here quantified.

6. Conclusion

Although the area of the Ucayali’s 1984-2019 meander belt represents only a small fraction of the Amazonian basin area, it significantly contributes to the amount of C that is transferred from the floodplain forest to the aquatic continuum. The amount of woody C per unit area provided by floodplain erosion caused by lateral channel erosion is nearly ten-fold higher than that provided by central Amazon wetlands. Extrapolation of our results suggests that free meandering white-water rivers may act as major agent in the global C cycle. These findings point to the importance to quantify the overall contribution of free meandering forested floodplain rivers worldwide to the global C cycle. In addition to variations in channel migration rates, different floodplain tree species may show contrasting C-stock potentials and related forest carbon export rates according to climate zones and biogeographical regions.

7. Author contributions

Romain Wacker: Conceptualization, Methodology, Formal analysis, Writing- Original draft preparation. **Dov Corenblit:** Original Idea, Supervision, Conceptualization, Writing- Original draft preparation. **Frédéric Julien**: Writing - Review & Editing. **Jean-Michel Martinez**: Writing - Review & Editing. **Johannes Steiger***:* Writing - Review & Editing.

8. Competing interest statement

The authors have no competing interests to declare.

9. Acknowledgements

RW acknowledges financial support from the French National Research Agency through an Investissement d’Avenir (Labex CEBA, ref. ANR-10-LABX-25-01).

10. References

Abril, G., Martinez, J.-M., Artigas, L. F., Moreira-Turcq, P., Benedetti, M. F., Vidal, L., Meziane, T., Kim, J.-H., Bernardes, M. C., Savoye, N., Deborde, J., Souza, E. L., Albéric, P., Landim de Souza, M. F., & Roland, F. (2014). Amazon River carbon dioxide outgassing fuelled by wetlands. *Nature* ***505***, 395–398. https://doi.org/10.1038/nature12797

Allen, J.R.L. (1965) A review of the origin and characteristics of recent alluvial sediments. *Sedimentology* **5**, 89-191.

Clark, K. E., Hilton, R. G., West, A. J., Malhi, Y., Gröcke, D. R., Bryant, C. L., Ascough, P. L., Robles Caceres, A., & New, M. (2013). New views on "old" carbon in the Amazon River: Insight from the source of organic carbon eroded from the Peruvian Andes. *Geochemistry, Geophysics, Geosystems* **14**, 1644–1659. https://doi.org/10.1002/ggge.20122

Constantine, J. A., Dunne, T., Ahmed, J., Legleiter, C., & Lazarus, E. D. (2014). Sediment supply as a driver of river meandering and floodplain evolution in the Amazon Basin. *Nature Geoscience* **7**, 899–903. https://doi.org/10.1038/ngeo2282

Drake, T. W., Raymond, P. A., Spencer, R. G. M. (2018) Terrestrial carbon inputs to inland waters: A current synthesis of estimates and uncertainty. *Limnology and Oceanography Letters* **3**, 123–142. https:// doi.org/10.1002/lol2.10055

Feng, X., Feakins, S. J., Liu, Z., Ponton, C., Wang, R. Z., Karkabi, E., Galy, V., Berelson, W. M., Nottingham, A. T., Meir, P., & West, A. J. (2016). Source to sink: Evolution of lignin composition in the Madre de Dios River system with connection to the Amazon basin and offshore. *Journal of Geophysical Research : Biogeosciences* **121**, 1316–1338. https://doi.org/10.1002/2016JG003323

Filoso, S., Williams, M. R., & Melack, J. M. (1999). Composition and deposition of throughfall in a flooded forest archipelago. *Biogeochemistry* **45**, 169–195. https://doi.org/10.1023/A:1006108618196

Finer M, Jenkins CN (2012) Proliferation of Hydroelectric Dams in the Andean Amazon and Implications for Andes-Amazon Connectivity. PLoS ONE 7(4): e35126. https://doi.org/10.1371/journal.pone.0035126

Galy, V., Peucker-Ehrenbrink, B., & Eglinton, T. (2015). Global carbon export from the terrestrial biosphere controlled by erosion. *Nature* **521**, 204–207. https://doi.org/10.1038/nature14400

Gorelick, N., Hancher, M., Dixon, M., Ilyushchenko, S., Thau, D., & Moore, R. (2017). Google Earth Engine: Planetary-scale geospatial analysis for everyone. *Remote Sensing of Environment* **202**, 18–27. https://doi.org/10.1016/j.rse.2017.06.031

Hoffmann, T., Glatzel, S., & Dikau, R. (2009). A carbon storage perspective on alluvial sediment storage in the Rhine catchment. *Geomorphology*, **108**, 127–137. https://doi.org/10.1016/j.geomorph.2007.11.015

HYBAM, www.sno-hybam.org, last access at 01/12/2020.

Junk, W. J. (1985). The Amazon floodplain–a sink or source for organic carbon. Mitteilungen aus dem Geologische-Palaontologischen Institut der Universitat Hamburg. SCOPE/UNEP Sonderband **58**, 267–283.

Junk, Wolfgang J., Bayley, Peter B., Sparks, R. (1989). The flood pulse concept in river-floodplain systems. In *Canadian Journal of Fisheries and Aquatic Science*, **106**, 10–127.

Kalliola, R., Salo, J., Puhakka, M., & Rajasilta, M. (1991). New Site Formation and Colonizing Vegetation in Primary Succession on the Western Amazon Floodplains. *The Journal of Ecology* **79**, 877–901. https://doi.org/10.2307/2261087

Kalliola, R., Salo, J., Puhakka, M., Rajasilta, M., Häme, T., Neller, R.J., E. Räsänen M.E., & Danjoy Aria, W.A. (1992) Upper Amazon channel migration: implications for vegetation disturbance and succession using bitemporal Landsat MSS images. *Naturwissenschaften* **79**, 75–79.

Lamotte, S. (1990). Fluvial dynamics and succession in the Lower Ucayali River basin, Peruvian Amazonia. *Forest Ecology and Management* **33**, 141–156.

Ielpi, A., Lapôtre, M. G. A. (2019) A tenfold slowdown in river meander migration driven by plant life. *Nature Geoscience* **13**, 82–86. https://doi.org/10.1038/s41561-019-0491-7

Leopold, L.B. & Wolman, M.G. (1960) River meanders. *Geologicla Society of America Bulletin* **71**, 769-794.

Mayorga, E., Aufdenkampe, A. K., Masiello, C. A., Krusche, A. V., Hedges, J. I., Quay, P. D., Richey, J. E., & Brown, T. A. (2005). Young organic matter as a source of carbon dioxide outgassing from Amazonian rivers. *Nature* **436**, 538–541. https://doi.org/10.1038/nature03880

McClain, M. E., & Naiman, R. J. (2008). Andean influences on the biogeochemistry and ecology of the Amazon River. *BioScience* **58**, 325–338. https://doi.org/10.1641/B580408

Mertes, L. A. K., Daniel, D. L., Melack, J. M., Nelson, B., Martinelli, L. A., & Forsberg, B. R. (1995). Spatial patterns of hydrology, geomorphology, and vegetation on the floodplain of the Amazon river in Brazil from a remote sensing perspective. *Geomorphology* **13**, 215-232 https://doi.org/10.1016/0169-555X(95)00038-7

Neu, V., Ward, N. D., Krusche, A. V., & Neill, C. (2016). Dissolved organic and inorganic carbon flow paths in an amazonian transitional forest. *Frontiers in Marine Science* **3** https://doi.org/10.3389/fmars.2016.00114

Peixoto, J. M. A., Nelson, B. W., Wittmann, F. (2009) Spatial and temporal dynamics of river channel migration and vegetation in centralAmazonian white-water floodplains by remote-sensing techniques. *Remote Sensing of Environment* **113**, 2258–2266. http://dx.doi.org/10.1016/j.rse.2009.06.015

Pekel, J. F., Cottam, A., Gorelick, N., & Belward, A. S. (2016). High-resolution mapping of global surface water and its long-term changes. *Nature* **540**, 418–422. https://doi.org/10.1038/nature20584

Puhakka, M., Kalliola, R., Rajasilta, M., & Salo, J. (1992). River Types, Site Evolution and Successional Vegetation Patterns in Peruvian Amazonia. *Journal of Biogeography*. https://doi.org/10.2307/2845707

Raymond, P. A., Hartmann, J., Lauerwald, R., Sobek, S., McDonald, C., Hoover, M., Butman, D., Striegl, R., Mayorga, E., Humborg, C., Kortelainen, P., Dürr, H., Meybeck, M., Ciais, P., & Guth, P. (2013). Global carbon dioxide emissions from inland waters. *Nature* **503**, 355–359. https://doi.org/10.1038/nature12760

Richey, J. E., Brock, J. T., Naiman, R. J., Wissmar, R. C., & Stallard, R. F. (1980). Organic carbon: oxidation and transport in the Amazon River. *Science* **207**, 1348-1351. https://doi.org/10.1126/science.207.4437.1348

Salo, J., Kalliola, R., Häkkinen, I., Mäkinen, Y., Niemelä, P., Puhakka, M., & Coley, P. D. (1986). River dynamics and the diversity of Amazon lowland forest. *Nature* **322**, 254–258. https://doi.org/10.1038/322254a0

Salo, J., & Räsänen, M. (1989). Hierarchy of landscape patterns in western Amazon. In: Holm-Nielsen, L.B., Nielsen, I.C., Balslev, H. (eds) Tropical forests: Botanical dynamics, speciation and diversity, Academic Press, London.

Santini, W., Camenen, B., Le Coz, J., Vauchel, P., Guyot, J. L., Lavado, W., Villar, R. E., Julien F. & Martinez J.M. (2019). An index concentration method for suspended load monitoring in large rivers of the Amazonian foreland. *Earth Surface Dynamics* **7**, 515-536. https://doi.org/10.5194/esurf-7-515-2019

Sawakuchi, H. O., Neu, V., Ward, N. D., Barros, M. de L. C., Valerio, A. M., Gagne-Maynard, W., Cunha, A. C., Less, D. F. S., Diniz, J. E. M., Brito, D. C., Krusche, A. V., & Richey, J. E. (2017). Carbon dioxide emissions along the lower Amazon River. *Frontiers in Marine Science* **4**. https://doi.org/10.3389/fmars.2017.00076

Schöngart J., Wittmann F. (2010) Biomass and Net Primary Production of Central Amazonian Floodplain Forests. In: Junk W., Piedade M., Wittmann F., Schöngart J., Parolin P. (eds) Amazonian Floodplain Forests. Ecological Studies (Analysis and Synthesis), vol 210. Springer, Dordrecht. https://doi.org/10.1007/978-90-481-8725-6_18

Schwenk, J., Khandelwal, A., Fratkin, M., Kumar, V., & Foufoula-Georgiou, E. (2017). High spatiotemporal resolution of river planform dynamics from landsat: The rivMAP toolbox and results from the Ucayali river. *Earth and Space Science* **4**, 46–75. https://doi.org/10.1002/2016EA000196

Spencer, R. G. M., Aiken, G. R., Dornblaser, M. M., Butler, K. D., Holmes, R. M., Fiske, G., Mann, P. J., Stubbins, A. (2013) Chromophoric dissolved organic matter export from US rivers. *Geophysical Research Letters* **40**, 1575–1579. https://doi.org/10.1002/grl.50357

Sutfin, N. A., Wohl, E. E., & Dwire, K. A. (2016). Banking carbon: A review of organic carbon storage and physical factors influencing retention in floodplains and riparian ecosystems. *Earth Surface Processes and Landforms* **41**, 38–60. https://doi.org/10.1002/esp.3857

Torres, M. A., Limaye, A. B., Ganti, V., Lamb, M. P., West, A. J., Fischer, W. W. (2017) Model predictions of long-lived storage of organiccarbon in river deposits. *Earth Surface Dynamics* **5**, 711–730. https://doi.org/10.5194/esurf-5-711-2017

Ward, N. D., Bianchi, T. S., Medeiros, P. M., Seidel, M., Richey, J. E., Keil, R. G., & Sawakuchi, H. O. (2017). Where Carbon Goes When Water Flows: Carbon Cycling across the Aquatic Continuum. *Frontiers in Marine Science* **4**. https://doi.org/10.3389/fmars.2017.00007

Ward, N. D., Keil, R. G., Medeiros, P. M., Brito, D. C., Cunha, A. C., Dittmar, T., Yager, P. L., Krusche, A. V., & Richey, J. E. (2013). Degradation of terrestrially derived macromolecules in the Amazon River. *Nature Geoscience* **6**, 530–533. https://doi.org/10.1038/ngeo1817

Wohl, E., & Ogden, F. L. (2013). Organic carbon export in the form of wood during an extreme tropical storm, Upper Rio Chagres, Panama. *Earth Surface Processes and Landforms*, **38**, 1407–1416. https://doi.org/10.1002/esp.3389

Wohl, E., Dwire, K., Sutfin, N., Polvi, L., & Bazan, R. (2012). Mechanisms of carbon storage in mountainous headwater rivers. *Nature communications* **3**, 1–8.

11. Tables and figures

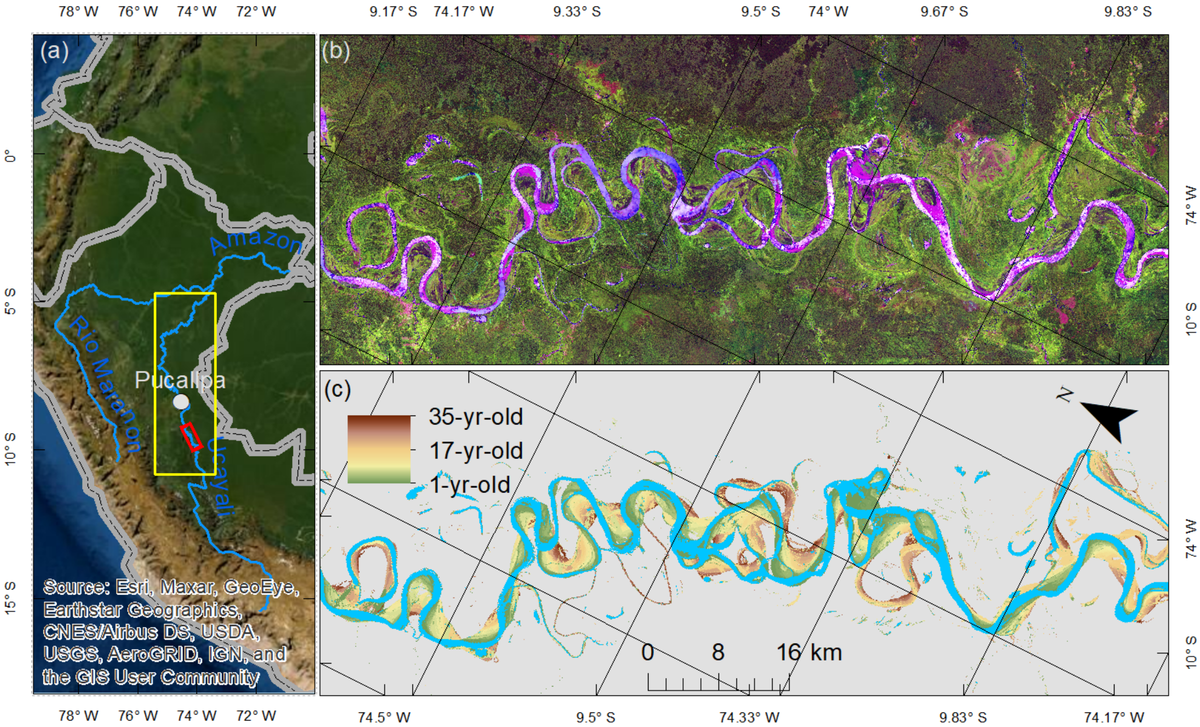

Figure 1 The freely meandering Ucayali River in the upper Amazonian region, Peru. **(a)** Location map: the yellow rectangle indicates the extent of the study area and the red rectangle indicates the extensions of panels (b) and (c), located approximately 120 km upstream of Pucallpa, Peru. **(b)** False colour composite satellite image showing the Ucayali meander belt extension in light green. This cloud-free satellite Landsat 8 image was obtained through the selection of the greenest pixels over the year 2018. The first short wave infra-red satellite band was affected to the red colour on screen, the near infra-red band to the green and the red band to the blue. **(c)** Floodplain ages range from 1-year (green colour) to 35-year (brown colour) within the 1984-2019 meander belt. Blue and grey colours correspond respectively to surface water and upland areas formed before 1984 (non-determined ages), respectively.

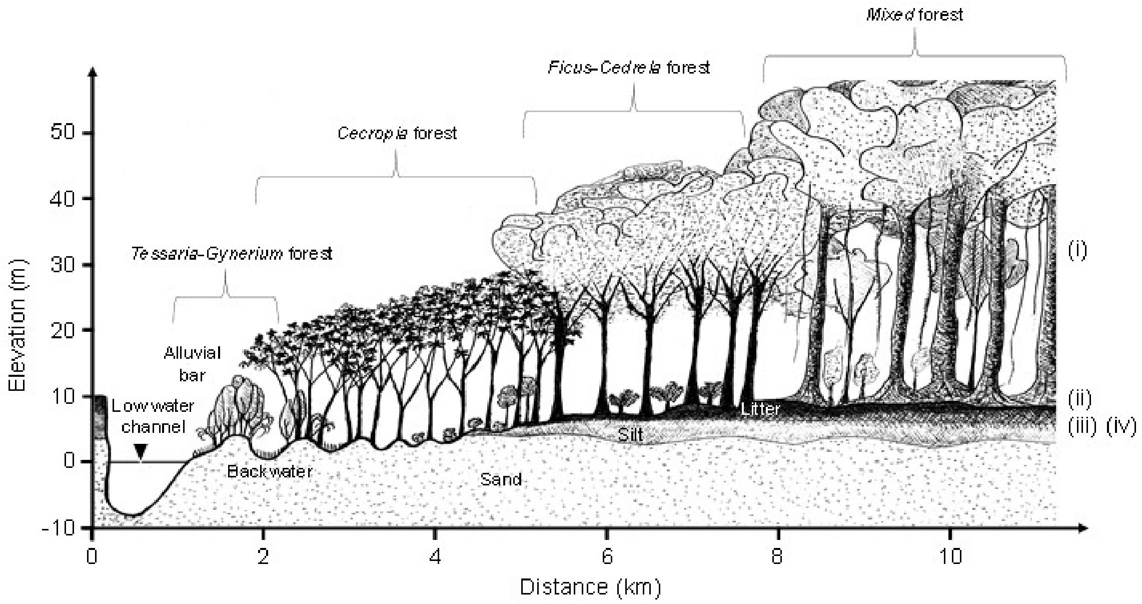

Figure 2 Simplified model of the floodplain vegetation succession in the study area which comprises four main interrelated carbon reservoirs (modified from Salo *et al.*, 1986; Kayranli *et al*., 2010; Stufin *et al*., 2016): (i) aboveground living terrestrial and seasonally flooded forest biomass (trunk, branches and foliage); (ii) aboveground necromass (dead wood and litter); (iii) belowground living biomass (roots and micro-organisms); and (iv) total organic matter in the soil (decomposed dead organic flora and fauna). The present study focused on the first carbon reservoir of the floodplain, i.e. aboveground living terrestrial and seasonally flooded forest biomass.

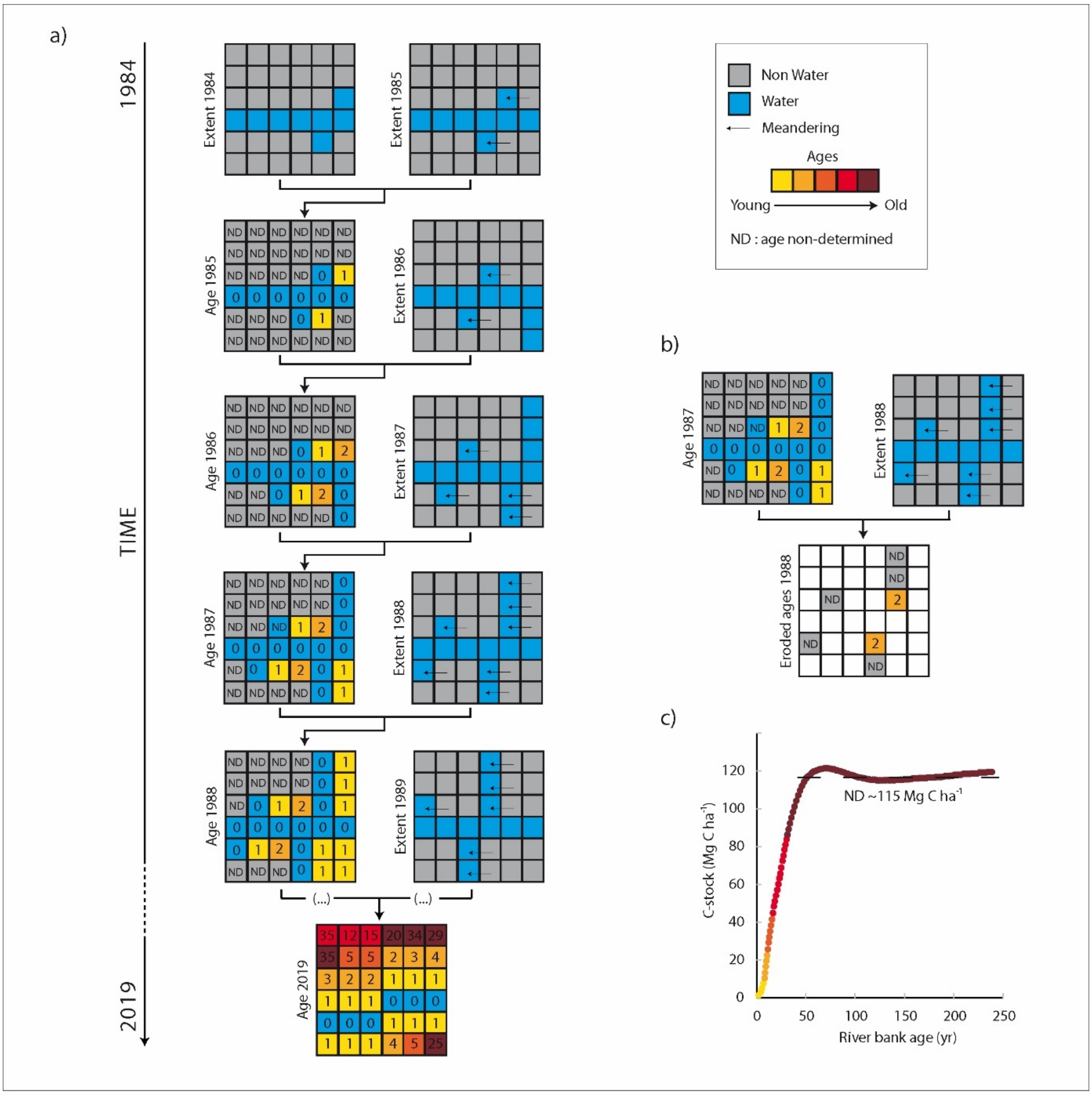

Figure 3 Conceptual approach used to derive forest above ground carbon stock (C-stock) from floodplain area age. **a)** Pixel-by-pixel and year-by-year algorithm used to obtain yearly maps of area ages based on the analysis of the yearly water classification history dataset (Pekel *et al.*, 2016). **b)** Pixel-by-pixel and year-by-year algorithm used to obtain yearly maps of eroded floodplain area ages. **c)** Data series used to model and derive C-stocks from floodplain area ages (Schöngart and Wittmann, 2010).

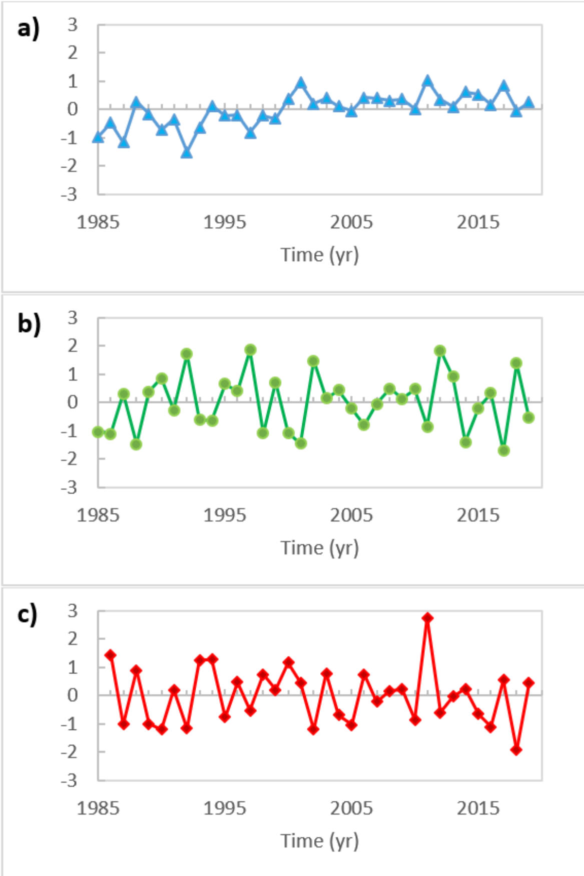

Figure 4 Annual area fluctuations of **a)** water surfaces, **b)** floodplain formation and **c)** floodplain erosion between 1984 and 2019. Values are standardized, i.e. the 1984-2019 average was subtracted and the result was divided by the 1984-2019 standard deviation.

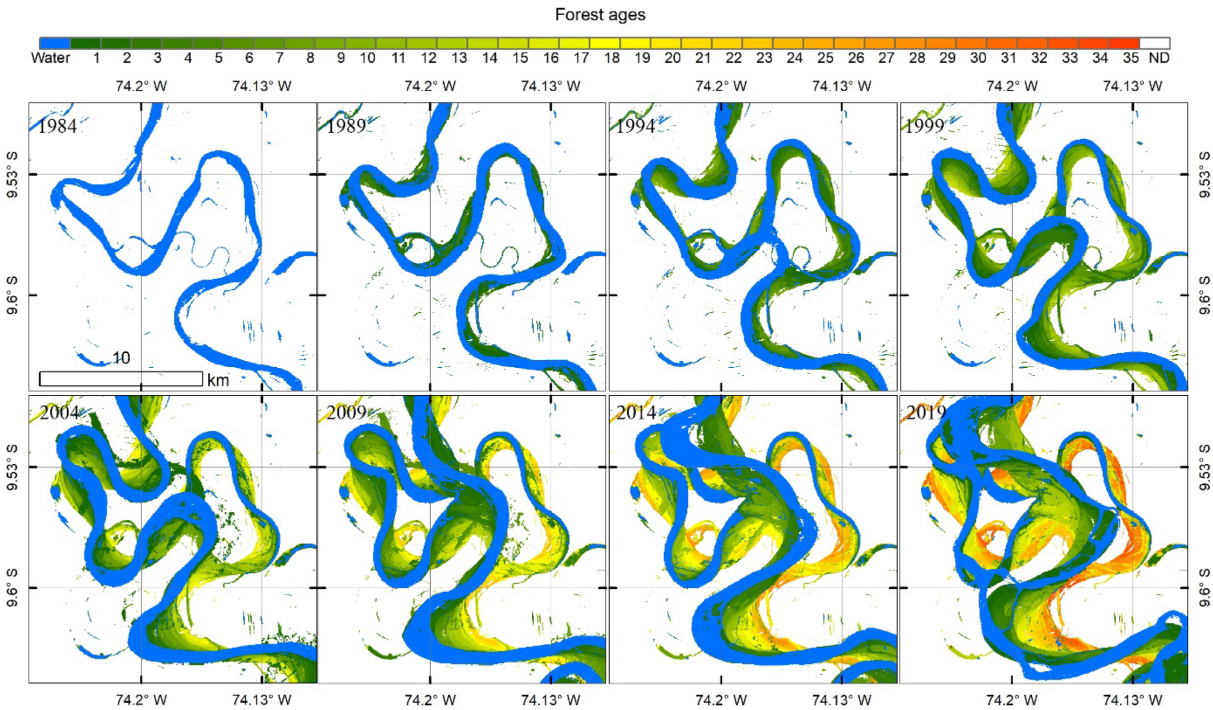

Figure 5 River meandering and floodplain forest dynamics according to a 5-yr time interval between 1984 and 2019 in the vicinity of Sampaya (Peru). Annual maps were created using the algorithm described in Fig. 3a. Non-eroded, remaining floodplain and upland forests which established before 1984 are indicated as age non-determined (ND; white colour).

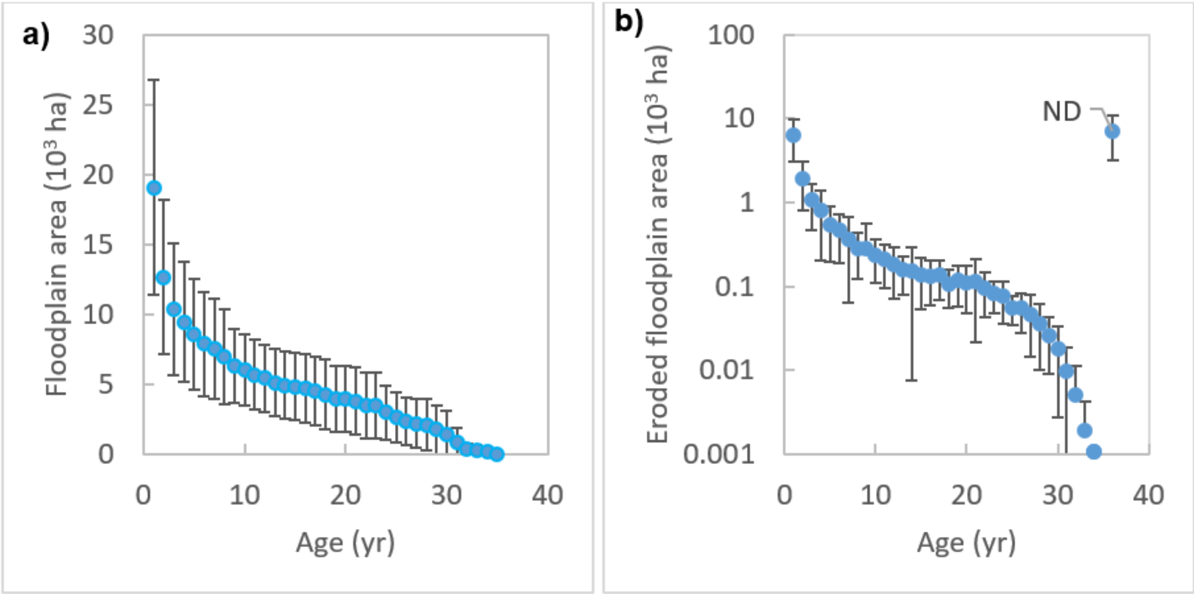

Figure 6 Age structure of vegetated floodplain areas observed in the 1984-2019 active meander belt. **a)** Floodplain areas according to floodplain ages established since 1984. **b)** Eroded floodplain areas since 1984 according to floodplain ages. Non-determined ages (ND) corresponding to floodplain or upland areas established before 1984, were considered for erosion. Together, mean annual erosion accounted for $19.8\pm6.7\times10^3$ ha^{-1} yr^{-1}. Points and bars indicate annual mean values for the period 1984-2019 and their standard deviations, respectively.

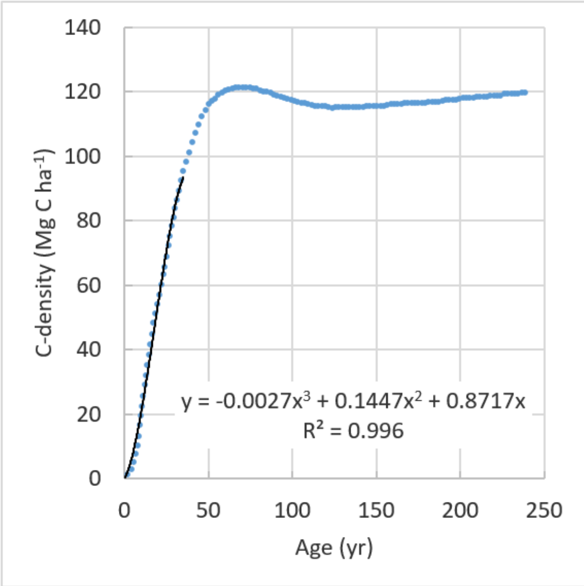

Figure 7 Model used to derive above-ground forest C-stocks from floodplain forest age. The model between 1 and 35 years (3rd polynomial; black line) is based on data (dots) published by Schöngart and Wittman (2010). The data error range is ±2% (not indicated in the figure).

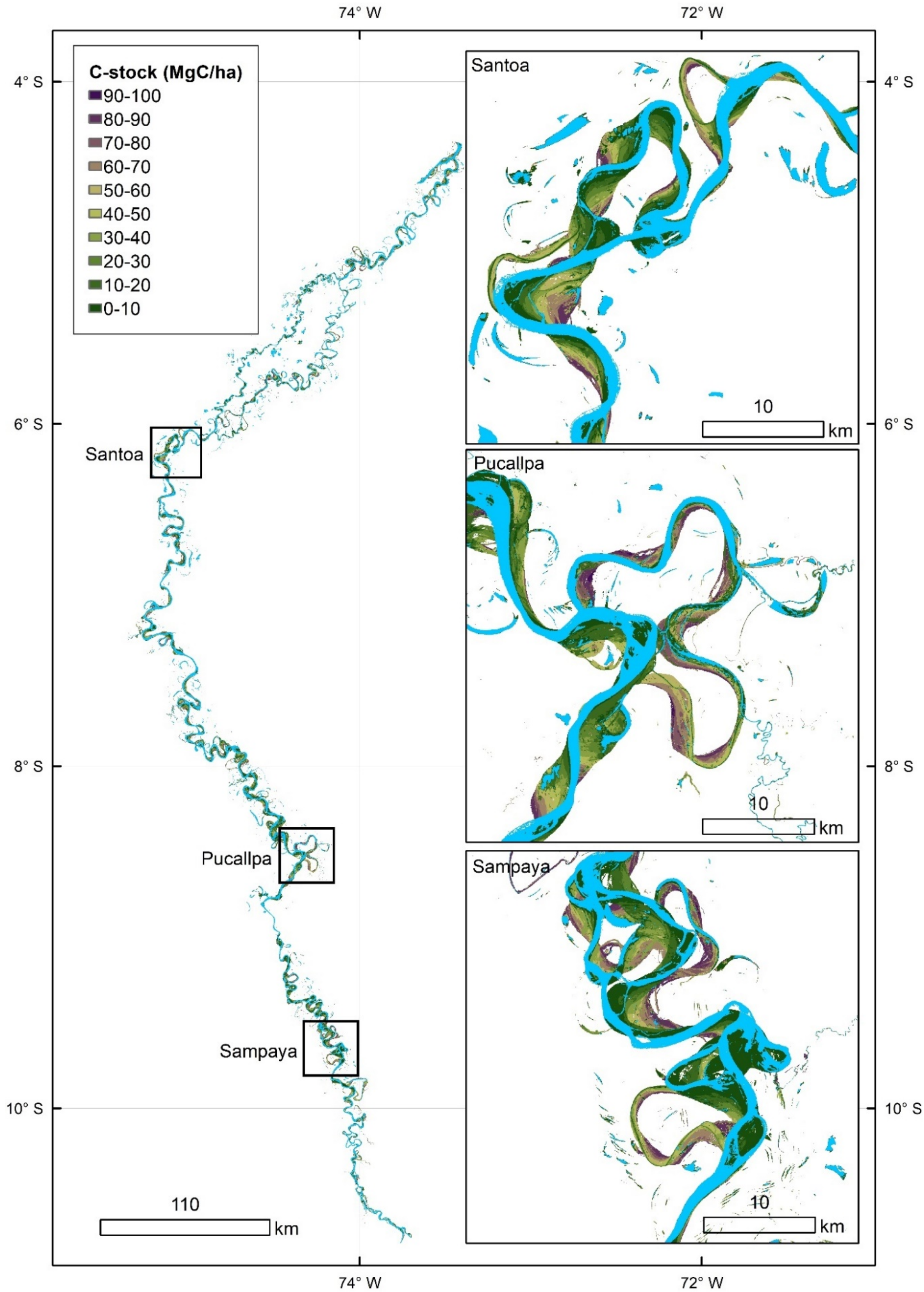

Figure 8 Above-ground floodplain forest carbon stock (C-stock in Mg C ha^{-1}) in the Ucayali 1984-2019 meander belt. Thirty yearly maps were produced for the 1984-2019 period. This figure shows the map of 2019.

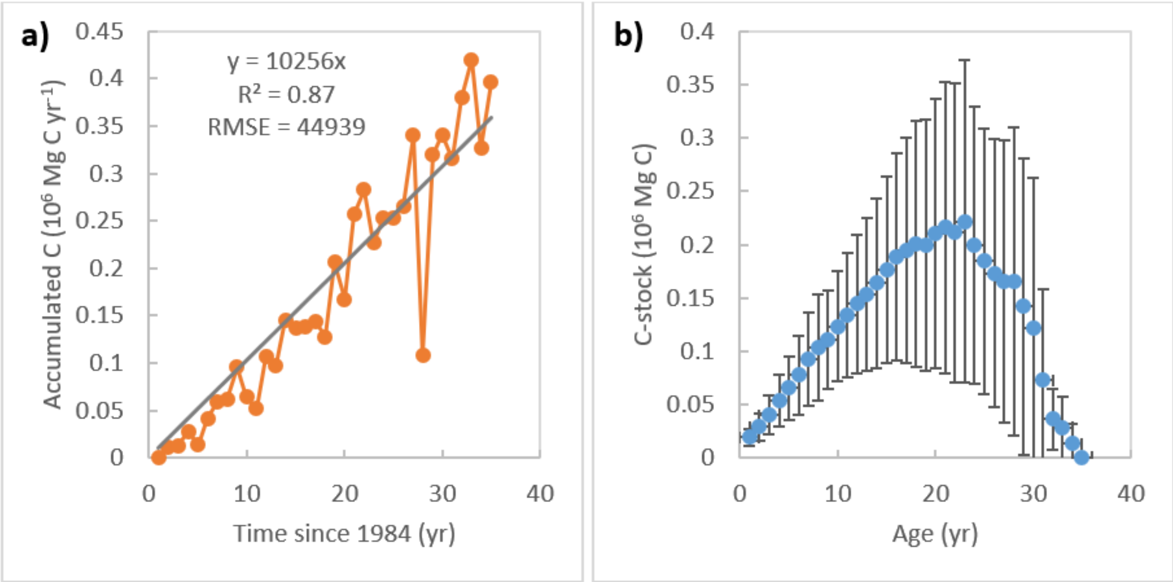

Figure 9 Floodplain forest carbon stocks (C-stocks) during the 1984-2019 period in the Ucayali active meander belt. **a)** Annual C accumulation in the floodplain forest established since 1984 and quantified annually until 2019. The black line indicates the annual C accumulation rate as a linear trend of 10256 Mg C yr^{-1} ($R^2 = 0.87$, p value < 0.01 and RMSE = 44939 Mg C yr^{-1}). **b)** Annual C-stock accumulated in the floodplain forest according to the floodplain age established since 1984.

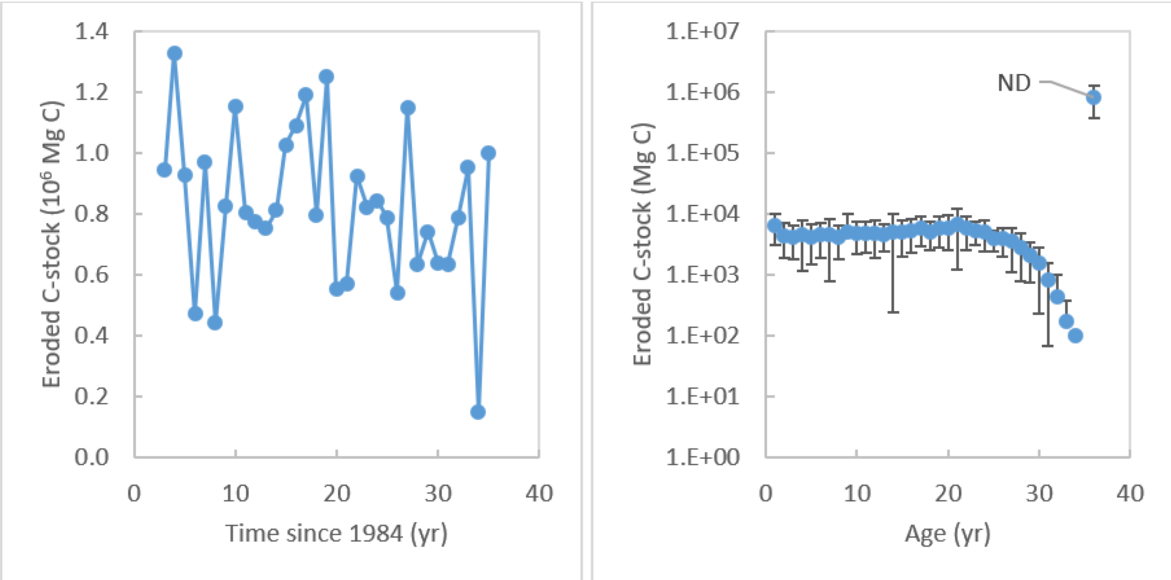

Figure 10 Erosion of floodplain forest carbon stocks (C-stocks) caused by lateral channel migration. **a)** Annual C-stocks eroded from the floodplain forest during lateral channel migration between 1984 and 2019. **b)** Annual C-stock eroded from the floodplain forest during lateral channel migration according to forest age. ND indicates floodplain and upland forests established before 1984.